JOURNAL OF CATALYSIS **177,** 1–10 (1998)
ARTICLE NO. CA982050

The Relationship between the Structure and Activity of Nanometer Size Gold When Supported on $Mg(OH)_2$

D. A. H. Cunningham,* W. Vogel,† H. Kageyama,* S. Tsubota,* and M. Haruta*,[1]

*Osaka National Research Institute, Midorigaoka 1, Ikeda City, Osaka 563, Japan; and †Fritz Haber Institut der Max-Plank-Gesellschaft, Faradayweg 4-6, D14195 Berlin (Dahlem), Germany

Received April 22, 1997; revised December 2, 1997; accepted February 23, 1998

In the following paper catalysts of Au supported on $Mg(OH)_2$ were analyzed by extended X-ray absorption fine structure spectroscopy and Debye function analysis. From these studies only catalysts with Au-size distributions below 1 nm in size were found to be active for CO oxidation. Below 1 nm in size the gold exists in two forms; icosahedral and fcc cuboctahedral. Comparison of turnover frequencies for catalysts prepared with different ratios of the two symmetries suggest that the icosahedral symmetry is the more active form. Above 1 nm in size the gold takes either FCC cuboctahedral or decahedral symmetry. These results suggest that oxidation of CO over the Au/$Mg(OH)_2$ catalyst is structure-dependent and that care must be taken in comparing results, where no structural information is available.

1. INTRODUCTION

In contrast to the inert nature of the bulk metal, nano-size particles of Au often show high and unusual catalytic activities. For example, compared to platinum, nano-size gold is far more active for the oxidation of certain compounds, such as CO (1–4). Also, when gold is supported on TiO_2, the catalyst is uniquely able to selectively oxidize and reduce alkenes, with the reaction switching from oxidation to reduction at sizes 2 nm in size (5).

Analysis of ultra-small gold particles by EXAFS is usually hindered by the inhomogeneous nature of the sample being studied. Because of the wide dispersion of different particles that can exist on the support surface, it is often impractical to isolate the origin of one specific signal from the background noise. This problem is made worse by the number average dependency of the EXAFS technique, which means that even if the majority of the particles are extremely small and contain less than a dozen or so atoms, a small number of large particles containing several hundred atoms can still make analysis impossible. For these reasons Debye function analysis (DFA), an X-ray diffraction technique, has recently become popular for the study of catalysts. The DFA techniques main advantage over EXAFS is the ability to analyze the crystal structure of the particle independently of the size distribution. As both sets of structural data, however, come from the same experimental diffraction pattern an internal check is made possible, allowing quite accurate information concerning the size distribution and their structure to be obtained (6–13).

Recent results obtained for Au/$Mg(OH)_2$ (14) which has the smallest known gold sizes, have shown the technique to be extremely useful in the study of particles that lie below the detection limit of transmission electron microscopy. In this study the reason for deactivation which occurs with time was found to be due to a gradual coalescence and transformation in the crystal structure of the supported gold to truncated decahedra. However, in the active gold catalyst there was a mixture of three different gold symmetries: icosahedral (15–22), fcc cuboctahedral, and truncated decahedral, which made a direct comparison between structure and catalytic activity very complex. In the following we therefore now attempt to build upon our previous work to try to identify which of the three symmetries is the most active for CO oxidation and to confirm whether or not gold clusters smaller than 13 atoms in size contribute to the overall activity.

2. EXPERIMENTAL

Au/$Mg(OH)_2$ catalysts with 5 wt% loading were prepared by standard deposition precipitation through dispersing ultra pure magnesia (Surface Area m/g, Ube industries Ltd.) in an aqueous solution of $HAuCl_4$ (23). To control the size distribution a saturated solution of magnesium citrate was then added slowly to the aqueous dispersion over a period of between 10 min to 1 h. The fast additions over 10-min periods typically gives rise to larger final size distributions upon calcination. During addition, as the $C_3H_7O_7^{3-}$ ion is able to directly reduce Au^{3+} to the metal state, care was also taken to maintain the pH

[1] Corresponding author.

0021-9517/98 $25.00

at around 9.6 during deposition. This is in order to control the release of the free citrate ion. After deposition all samples were washed thoroughly with distilled water to remove chlorine contaminants, filtered and dried overnight under vacuum. The catalyst is then obtained by calcination in air at temperatures between 80 and 400°C for between 60 to 180 min. Catalyst-containing concentrations of twinned fcc cuboctahedral gold were obtained by aging for 5 days in air before final calcination at 200°C. Blank $Mg(OH)_2$ supports for Debye function analysis studies (7, 8, 14) were prepared under identical conditions to those of the $Au/Mg(OH)_2$ catalyst with HCl used in place of $HAuCl_4$. All catalytic studies were carried out on a standard flow reactor using 0.100 to 0.15 g of catalyst (14).

The Debye function analysis method is based on the summation of the scattering vector components from model clusters of incremental increasing size. The summation is then compared directly with experimental X-ray diffraction data, obtained by a simple subtraction of the $Au/Mg(OH)_2$ spectra from the $Mg(OH)_2$ support. Free parameters are used for calculating the number fractions of the individual clusters, with additional parameters used to define the exponent of the Debye–Waller factor, the average d-spacing within the individual clusters and to account for errors in the background subtraction. Details of the method are given in Refs. (7, 8).

For DFA experiments translucent pellets of $Au/Mg(OH)_2$ catalyst and the $Mg(OH)_2$ support, $8 \times 15 \times 0.2\ mm^3$ in volume ($\mu d \approx 1.0$), were formed by pressing under a pressure of approximately 4 T/cm^2. The samples were then mounted in a specially designed reaction cell (10), which in turn was mounted on a commercial Guinier diffractometer (HUBER). The cell was aligned 45° to the transmission geometry. To aid background subtraction of the support, diffraction patterns of both the $Au/Mg(OH)_2$ catalyst and the $Mg(OH)_2$ support were taken simultaneously. X-rays of $CuK_{\alpha 1}$ wavelength were generated by a conventional X-ray source, with the energy defined using a Johansson-type Ge monochromator. Total surface exposures were calculated from DFA data by simply counting the number of surface atoms (N_s) of the model clusters used in the theoretical simulations. The total dispersion is the weight-averaged dispersion (N_s/N) of the individual model clusters (7). No assumption during this part of the analysis is made for blocking of part of the surface by bonding to the support.

In order to confirm that oxidic gold clusters smaller than 0.6 nm in size are inactive, EXAFS studies were carried out, one day after calcination, at room temperature (25°C). Data was recorded in transmission mode, at beamline 10B of the KEK synchrotron radiation source, Tsukuba Science City, Japan. For EXAFS studies only the slowly prepared $Au/Mg(OH)_2$ catalyst was analyzed. To determine the active species a total of six different calcination temperatures were used ranging from 80°C, which is well below the temperature at which Au becomes metallic, up to a final calcination temperature of 400°C. Between these two extremes, the gold contains varying amounts of nonmetallic Au, which is similar in structure to Au hydroxide, and a number of metallic gold species of varying Au–Au bond lengths. Because of the complexity of the obtained EXAFS signal, we decided not to use the EXAFS technique to determine the absolute structure of the gold, but, instead, as a fingerprint technique to follow the relative changes in percentage concentration of each of the species present. At 400°C the gold is entirely metallic and similar in nature to bulk gold. Activity studies for each sample were carried out on the same day as the EXAFS experiment. During data acquisition the storage ring was operated at 2.5 GeV with an average ring current of 250 mA. For energy selection a Si(311) monochromator was used. Background subtraction employed the Daresbury program EXBACK, with data analysis using the CERIUS^2 version of EXCURV92.

3. RESULTS AND DISCUSSION

It should be noted that, even though we have used a discrete set of model clusters in the DFA fitting routine, this does not actually imply their existence. A quasi-continuous distribution around discrete model size clusters, however, does reproduce quite well the observed experimental results and, as such, is considered to be a reasonable approximation of the actual gold size distribution present. It is also important to note that as the X-ray beam probes only the spherical average of the particle electron density, the DFA method is sensitive only to the intrinsic order of the crystal array, and not the particle morphology. As a result, although the Debye functions of the FCC cuboctahedral array differs substantially from icosahedra or decahedra, the Debye functions will be identical for two FCC crystals, even if they are of different particle shape. In other words, although we are able to distinguish between crystals of different symmetries, we cannot determine whether they exist in the form of a sphere or a raft.

Agreeing with previous published data (14), on comparing $Au/Mg(OH)_2$ catalysts, the highest measured activities were recorded for Au particles approaching 0.6 nm in size (Fig. 1). DFA-derived size distributions and measured catalytic conversions for selected $Au/Mg(OH)_2$ catalysts are shown in Table 1.

For calculating the absolute turnover frequency it is, however, necessary to know the total concentration of gold in the metal phase. At lower calcination temperatures, the slower rate of reduction of the gold hydroxide precursor usually means that a lower percentage of metallic gold phase will be present in the catalyst. To calculate the total percentage of metallic gold present we therefore carried

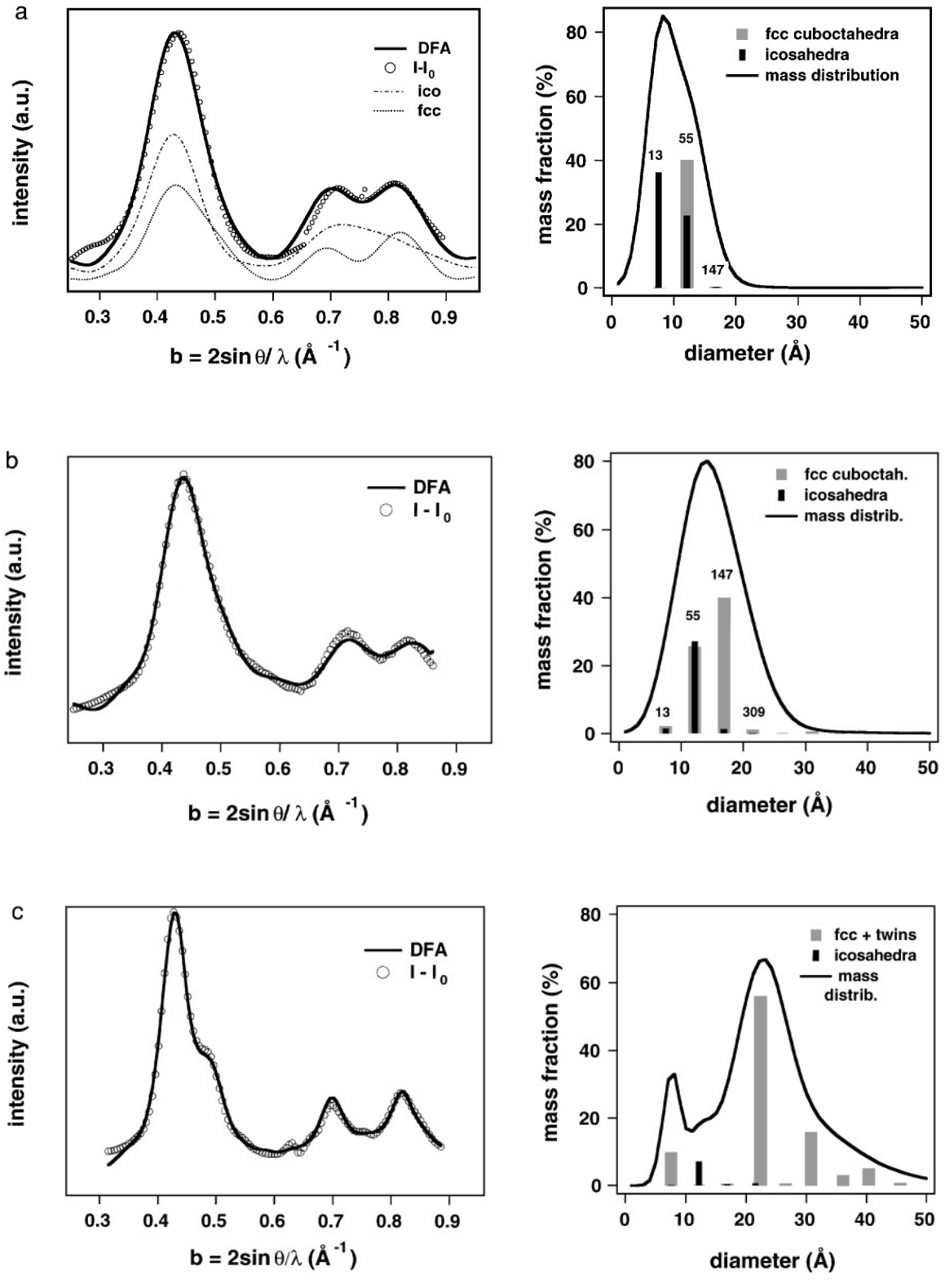

FIG. 1. Calculated X-ray intensity difference between Au/Mg(OH)$_2$ and Mg(OH)$_2$ support, with DFA simulations of particle size and symmetry for, from top to bottom: (a) slow deposition conditions and 280°C calcination; (b) fast deposition conditions and 280°C calcination; (c) fast deposition conditions and 5 day aging in air before final calcination at 200°C.

TABLE 1

Change in Activity and Turnover Frequency (TOF) with Changes in Particle Size

Catalyst preparation	Average size	Conversion (−70°C)	TOF (s^{-1})		
			Icosahedral	Fcc cuboct.	Combined
Slow addition 280°C	0.6–1.2 nm	100%	4.6×10^{-2}	7.3×10^{-2}	2.9×10^{-2}
Fast addition 200°C	0.7–2.1 nm	3–5%	1.8×10^{-2}	8×10^{-3}	5×10^{-3}
Fast addition 280°C	0.7–4.0 nm	4–6%	1.8×10^{-2}	2.1×10^{-3}	2×10^{-3}

Note. TOF's are given assuming all surface gold atoms assist CO oxidation (i.e., icosahedral and fcc combined), and for icosahedral and cuboctahedral particles in isolation. Larger particle sizes are generated by rapid addition of magnesium citrate and $HAuCl_4$ acid, during deposition precipitation.

out diffraction studies in the open slit mode (diffraction angle $22 \pm 1°$). In this way the degree of crystallization of the Au hydroxide can be calculated by the disappearance of the Au hydroxide peak. Careful analysis of the diffraction data shows that gold hydroxide begins to change to gold metal at a temperature of 180°C. At a calcination temperature of 200°C approximately 25% of the gold present is in the metallic phase (i.e., ≈1.25 wt%). By 280°C almost all the gold present has crystallized, suggesting that TOFs calculated using 5% loadings are more accurate at this temperature.

Total surface exposures and percentages of each symmetry type, used in the calculation of turnover frequencies, are presented in Table 2. Calculated lattice constants extend from 3.972 to 4.051 Å for rapidly prepared samples calcined at 200 and 280°C, respectively, and suggest contractions of between 0.7 and 2.6% from that of the bulk spacing. The total fraction of surface atoms belonging to the icosahedral symmetry is largest at 50% (0.58 × 86%) for catalysts prepared through a slow 1 h plus addition of gold chloroauric acid and magnesium citrate. In rapidly prepared catalysts calcined at 200 and 280°C, calculated percentages decrease to respectively 23 and 5.3%.

TABLE 2

Distribution of Icosahedral and FCC Cuboctahedral Particles by Mass Fraction for Catalyst Prepared under Different Deposition and Calcination Conditions

Catalyst preparation	Icosahedral		Cuboctahedral	
	Fraction	Surface %	Fraction	Surface %
Slow addition 280°C	0.58	86%	0.42	76%
Fast addition 200°C	0.30	77%	0.70	68%
Fast addition 280°C	0.07	76%	0.93	49%

Note. Total percentage of surface atoms of each symmetry type are as shown.

Using these values the turnover frequencies shown in Table 1 are obtained. Percentage conversions were recorded over a period of 3 h using 0.10 g catalyst, SV = 20,000 ml · hr^{-1} · g^{-1} · cat, at −70°C. In each case the composition of the reaction gas was 1% CO balanced in air. For the most active catalyst, which was 100% active at −70°C, a second study using 0.010 g of catalyst diluted in inert SiO_2 powder was carried out to obtain more accurate turnover frequencies. This reduced the conversion to 12%, from which a combined symmetry TOF of 2.9×10^{-2} events per second was calculated for this catalyst.

Also shown in Table 1 are the turnover frequencies based on the fraction of icosahedrals and fcc cuboctahedrals present, with the assumption that only one of the two symmetries contributes towards the activity. As turnover frequencies based on the individual symmetries are calculated using fewer surface atoms, the measured turnover frequencies shown for the individual symmetries are always higher than the combined TOF value.

From calculations based on the icosahedral content of both catalysts prepared by the fast addition of gold chloroauric acid and magnesium citrate, almost identical turnover frequencies at 1.8×10^{-2} events per second were obtained. Calculations based on the total number of surface icosahedral atoms present, therefore, appear to suggest a direct correlation between icosahedral content and activity. Such a conclusion is consistent with the fact that until now high conversions have only been observed in the $Au/Mg(OH)_2$ system when the gold particle size is predominately below 1 nm in size. This is the size region where the icosahedral symmetry first becomes thermodynamically more stable than fcc cuboctahedra. Calculations for the FCC cuboctahedral symmetry indicate that there is no correlation between turnover frequencies and observed percentage yields.

In detailed studies a major difference is, however, seen between catalysts containing between 13 to 55 atom icosahedral clusters and those containing only the larger clusters of around 55 atoms in size. Initially we assigned

this difference to different strengths of interaction between the gold and $Mg(OH)_2$ support. A second reason, however, and one which we find more reasonable given the greater understanding of the structure of the catalyst, is that this difference in TOF is due to the differences in Au–Au bonding which exists between particles of different size (Fig. 2). At small sizes, gold clusters containing 13 atoms lose the edge sites, resulting in a simplification of the electronic states of the gold cluster. This, we believe, results in the substantial difference in turnover frequencies which we observed between the highly active 13 atom size gold clusters and the slightly larger, but markedly less active cousins. This change in electronic binding is also thought to be responsible for the distinct changes in colour, from the dark red observed in the less active samples to the almost indescribable deep brownish maroon in the most active material. Changes in colour with size are common in gold and are thought to relate to the energy of the electrons contained in the 5d and 6s shells (24). However, there also exist slight changes in bond distances between the icosahedral and FCC cuboctahedral particles (21) which make a direct comparison between structure and colour almost impossible.

In all good mysteries, it is often the case that just as one believes that all the answers have been found, the less one suddenly becomes sure of the truth. Even considering only the icosahedral symmetry, which from activity studies appears to be the most active of the two symmetries present, one can define several possible sites for the oxidation of CO to CO_2. These can be classified into three main groups. The smallest are amorphous-like clusters that are either charged or uncharged between 1 to 12 atoms in size, icosahedral metallic particles of 13 atoms in size which are constructed entirely from corner apex sites, and finally, there exist metallic particles between 13 to 55 atoms in size which contain edge, step, kink, and/or face centered sites. In the latter case particles between 13 and 55 atoms in size are usually asymmetric in shape due to the irregular number of atoms contained.

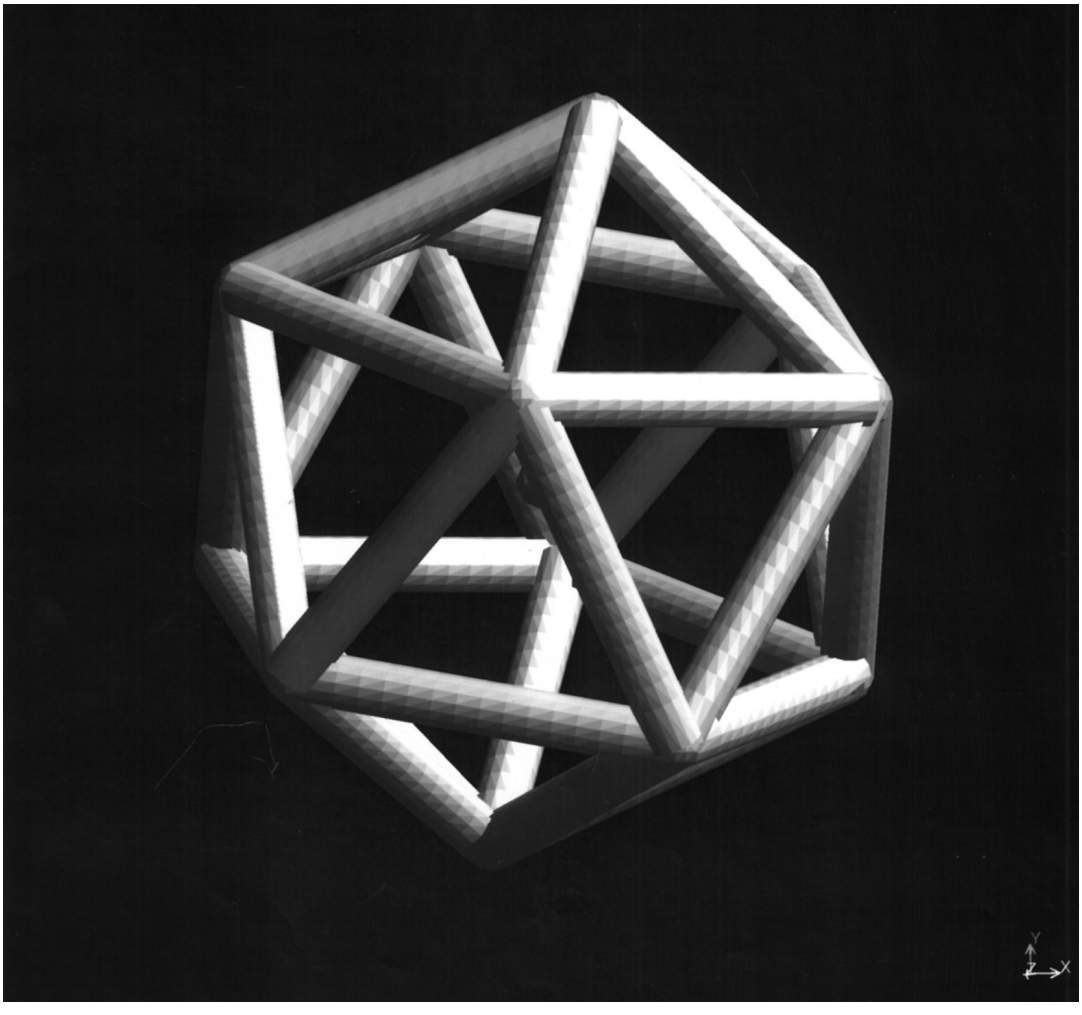

FIG. 2a. Molecular model diagrams of 13 atom icosahedral and fcc cuboctahedral gold. Fcc cuboctahedral symmetry is shown on the right.

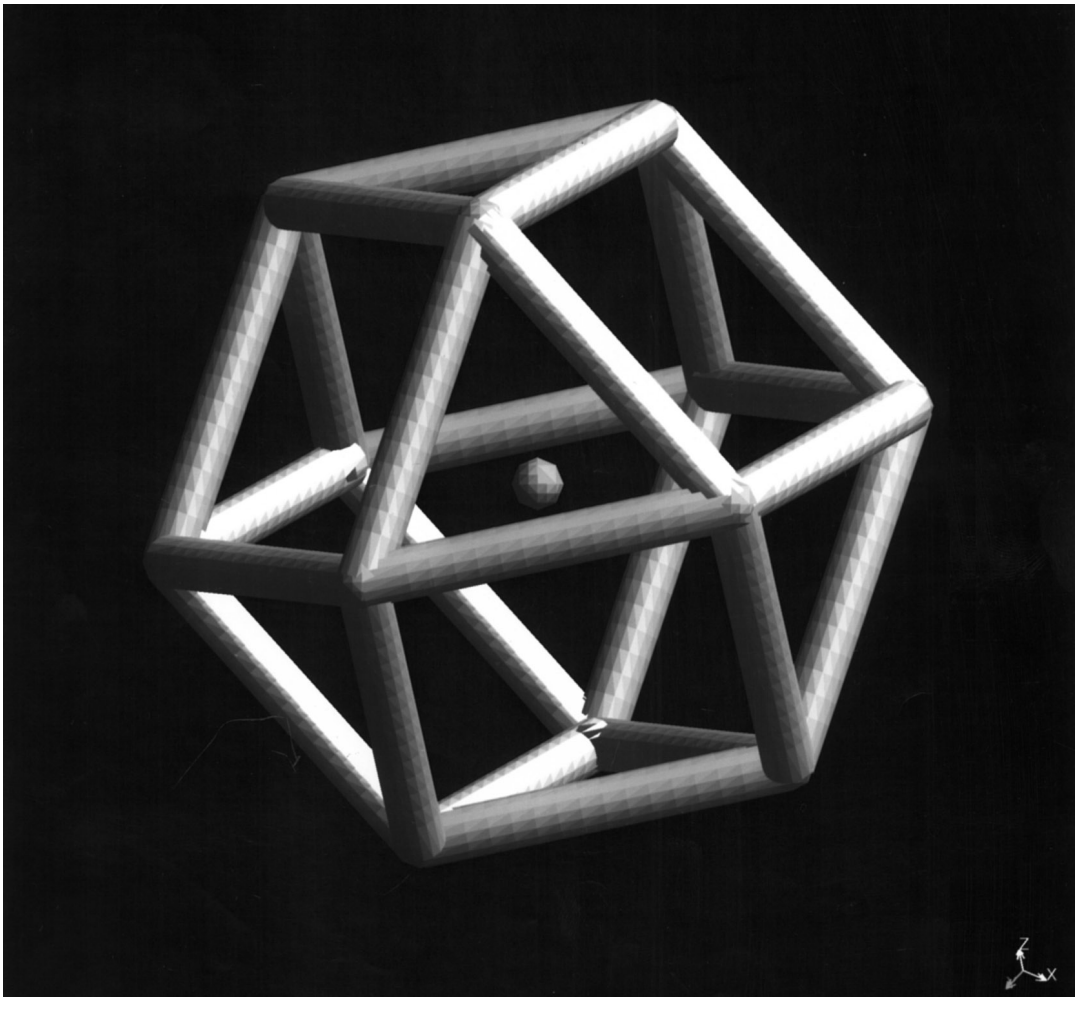

FIG. 2a—*Continued*

To obtain a clearer understanding of the size range over which CO oxidation is active we therefore carried out a simple series of experiments using EXAFS. By varying the calcination temperature of a $Au/Mg(OH)_2$ catalyst prepared under optimum conditions, it is possible to grow catalysts with varying ratios of particles of different sizes, which can then be identified from changes in the intensity of the Fourier transform. The Fourier transform is an offset radial distribution diagram of the atoms surrounding the central absorber and is calculated from the interference pattern of the X-ray photo-electron wave as it passes through the crystal media (25). As the Fourier transform is scaled to the coordination number this makes it possible to then visually determine changes in the chemical state through observing the changes in intensity.

At a calcination temperature of 80°C the Au is inactive and appears mono-dispersed and bound directly to oxygen; perhaps in the form of a hydroxide (refer to Fig. 3 and Table 3). On increasing the calcination temperature, decomposition of Au starts at 180°C and by 200°C one can clearly see the formation of Au–Au bonding with a mean interatomic bond-length of 2.41 Å. At present the origin of this peak remains unknown. It should be noted that as anharmonic effects are not included in these calculations; the bondlength obtained is much shorter than in reality; see Ref. (26). Nevertheless, anharmonicity included, such a short Au–Au bond implies oxidic and not metallic bonding between the gold. This is supported by the absence of any corresponding Au metal signal in the X-ray diffraction patterns and also by the presence of an intense peak (called the white line) at the rising part of the X-ray absorption edge (Fig. 4); the white line is a measure of the electron vacancy in the d-shell and increases with increasing oxidation state.

At calcination temperatures of 200°C, high activity for CO oxidation is observed for the first time, lasting 13 min at an operating temperature of −70°C (Table 4). Although this initially indicates that the oxidic Au–Au species at approximately 2.41 Å is partially active, the duration is extremely short, and it is considered more likely that the activity,

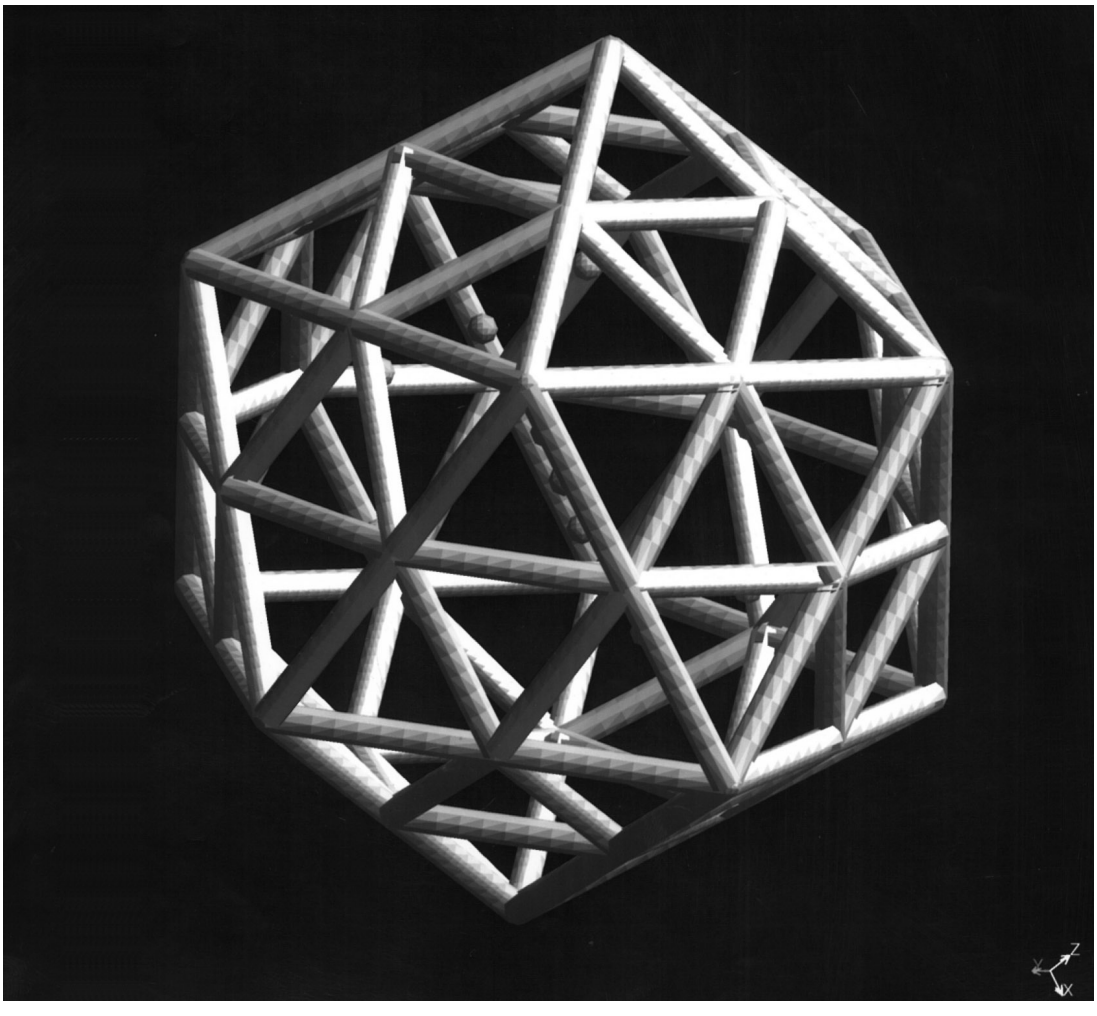

FIG. 2b. Molecular model diagrams of 55 atom icosahedral and fcc cuboctahedral gold. Fcc cuboctahedral symmetry is shown on the right.

instead, arises from trace amounts (<25%) of sub-nanometer metallic gold present in the media.

The initial doubt concerning the activity of the oxidic Au–Au species appears to be confirmed by studies at higher calcination temperatures. On increasing the calcination temperature, first to 250°C and then to 280°C, the concentration of oxidic gold decreases, as shown by the decrease in the Fourier transform and white line intensity at the X-ray adsorption edge (Fig. 4). Between 200 and 250°C, although the concentration of oxidic gold decreases, the activity increases. As this is the region where the content of sub-nanometer size gold contained in the catalyst is approximately the highest (14, 23), the increase in activity from 200 to 250°C must therefore arise entirely from the formation of metallic gold. In the Fourier transform this is seen by the formation of a distinct metallic type gold peak with a Au–Au bondlength of approximately 2.75 Å (27–31). This would imply a contraction of some 4.5% from bulk values, although again it should be noted that bondlengths of atoms in small clusters calculated by EXAFS are subject to error and cannot be considered reliable. The origin of the short Au–O bond with 1.63 Å bondlength, also seen in this table, is at present unknown but may relate to binding with the support.

At temperatures above 300°C the Au particles rapidly coalesce (ripen) due to a transition in the support from $Mg(OH)_2$ to MgO (Table 4) and the occupancy number approaches the value expected for Au bulk metal. The low Au–Au occupancy numbers observed at 2.75 Å in catalysts calcined between 250 to 280°C of 4 and 6.5, respectively, can easily be explained by the small size of the supported gold particle. Assuming that the Au particles are approximately 13 atoms in size, as shown in Fig. 2b, over 80% of all gold will be located at the surface and the predicted occupancy number should decrease to near 5 for fcc cuboctahedral symmetry, and to 6 for icosahedral symmetry, assuming that the surface geometry dominates the EXAFS signal. These values lie close to the obtained occupancy numbers of 4 at 250°C and 6.5 at 280°C and within the ±2 upper error of limit for the EXAFS technique (25). From

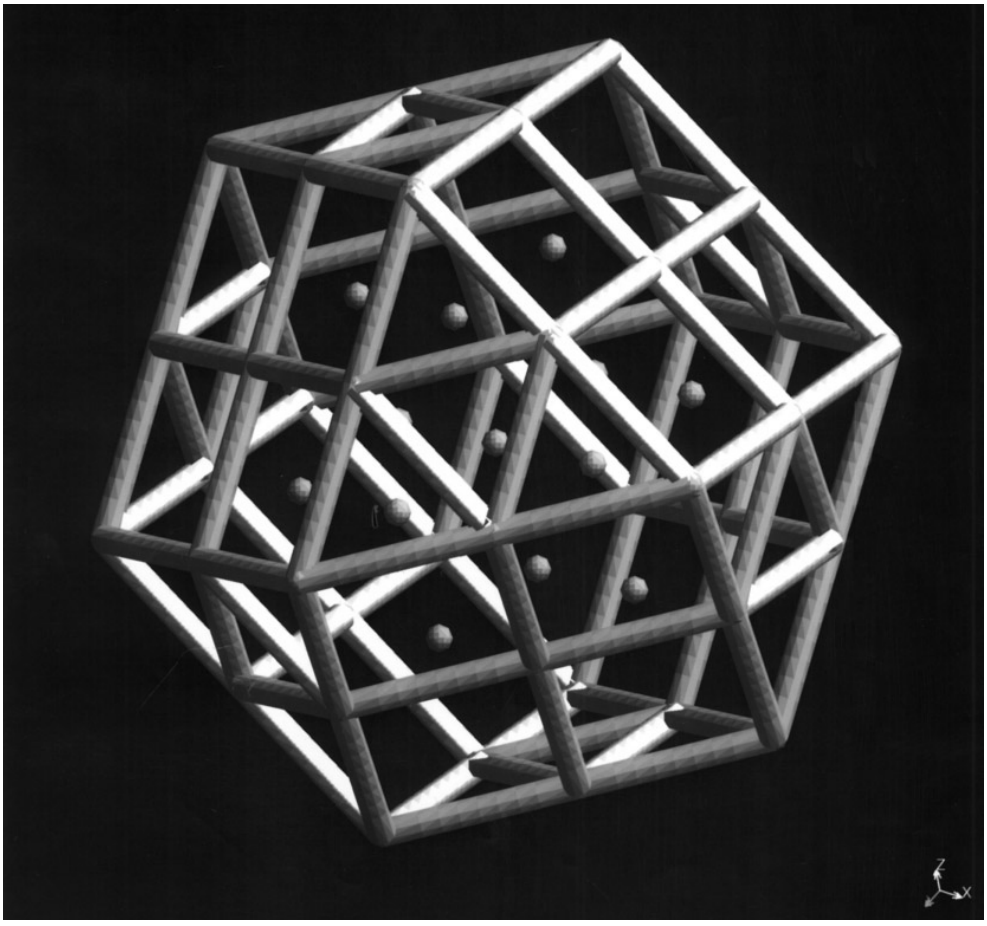

FIG. 2b—*Continued*

TABLE 3

Variation in the Calculated Occupancy Number, Atomic Distances, and Degree of Thermal Vibration of Atoms Surrounding Au with Increasing Calcination Temperature

Calcn temp/°C	Atom type	Coord. number	Bond distance	Thermal vibrat^{n}.
80°C	O	3.0	1.96	0.005
200°C	O	3.2	1.96	0.005
	Au	1.7	2.41	0.011
250°C	O	0.7	1.64	0.005
	O	3.3	1.93	0.006
	Au	2.1	2.41	0.015
	Au	4.0	2.76	0.022
280°C	O	0.9	1.63	0.003
	O	2.8	1.93	0.008
	Au	0.5	2.42	0.013
	Au	6.5	2.74	0.020
300°C	O	0.7	1.69	0.006
	O	2.2	1.97	0.008
	Au	1.4	2.45	0.015
	Au	10.4	2.83	0.025
400°C	Au	12	2.83	0.014

Note. All calcinations were carried out in air.

EXAFS results one can therefore determine that at a calcination temperature of 250°C, the mean particle size is most probably less than 1 nm and close to 13 atoms in size.

TABLE 4

Duration of 100% Conversion at −70°C over a Au/$Mg(OH)_2$ Catalyst Prepared under Optimum Deposition Conditions, as a Function of Calcination Temperature

Calcination temperature	Support structure	Metallic state	100% convers. at −70°C/min
80°C	$Mg(OH)_2$	Au hydroxide	Not active
200°C	$Mg(OH)_2$	Au fragments	13
250°C	$Mg(OH)_2$	Metal n.p. (0.6−1.0 nm)	>2000
280°C	$Mg(OH)_2$	Metal n.p. (0.6−1.2 nm)	960
300°C	$Mg(OH)_2$/MgO	Metal n.p. (3–5 nm)	Not active
400°C	MgO	Bulk metal	Not active

Note. Determination of the structure of the support and Au metal particle state was carried out by Debye function analysis. Metal n.p. refers to metal nano-particles.

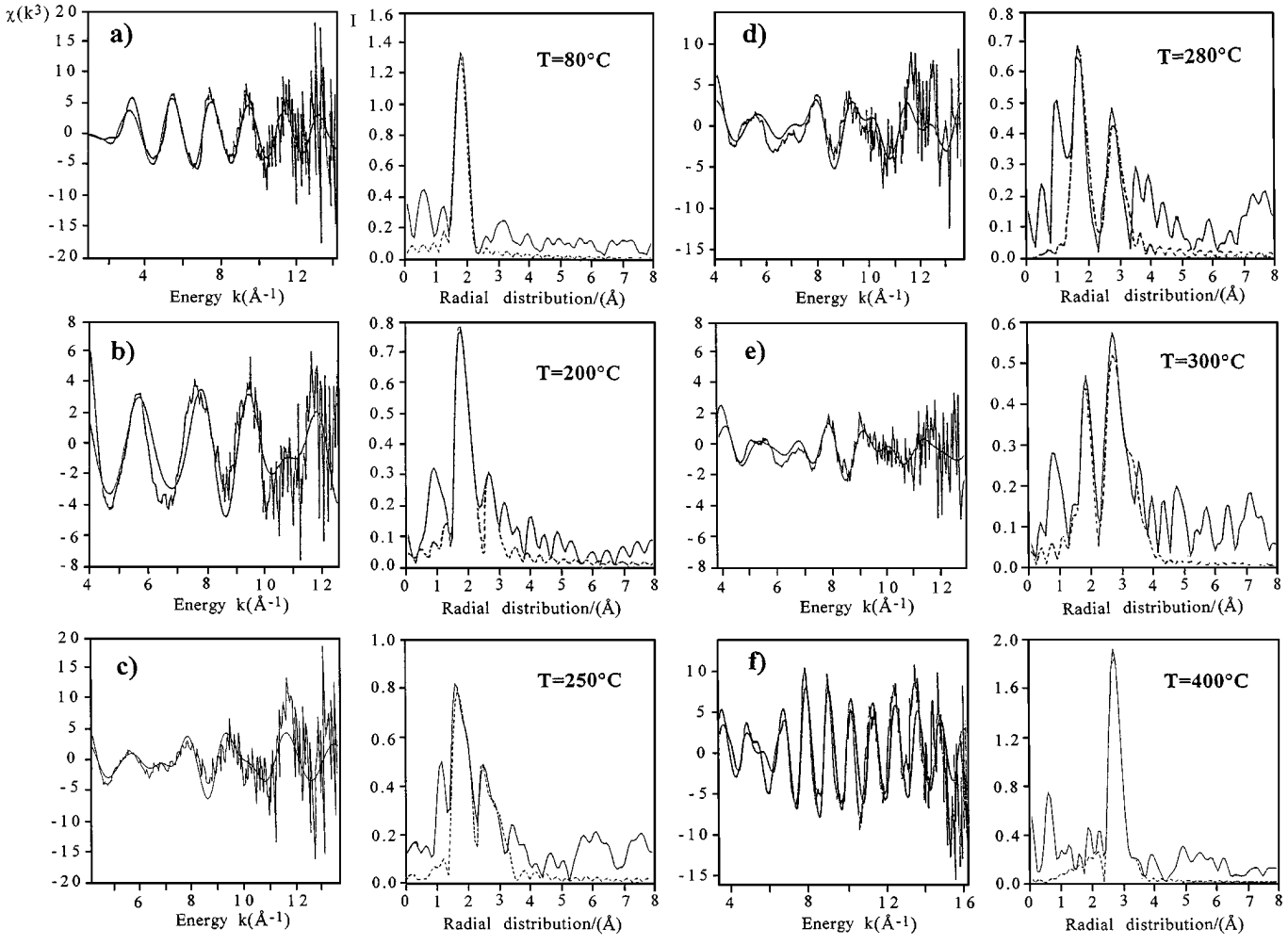

FIG. 3. Theoretical and experimental plots of the Au L_{III} edge EXAFS $\chi(K^3)$ weighted spectra and Fourier transform of Au/Mg(OH)$_2$ catalyst prepared under slow deposition conditions at calcination temperatures between 80 and 400°C. The Fourier transform is a radial distribution function showing the atom distribution surrounding the central gold.

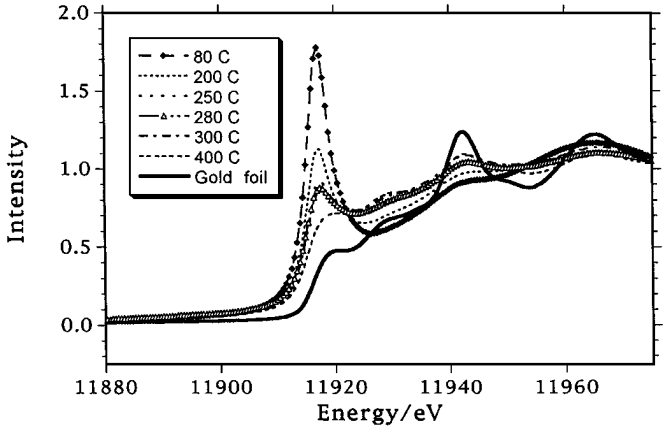

FIG. 4. X-ray L_{III} near edge spectra of Au/Mg(OH)$_2$ prepared under slow deposition conditions as a function of calcination temperature. All calcinations were carried out in air.

4. CONCLUSIONS

Catalysts of Au supported on Mg(OH)$_2$ were analyzed by extended X-ray absorption fine structure spectroscopy and Debye function analysis. Studies by DFA and EXAFS indicate that the active state of gold is icosahedral metal particles below 1 nm in size. Contractions in bond lengths of between 0.7 and 2.6% from bulk metal values were obtained from X-ray diffraction data. No major contribution to the activity could be detected for particles smaller than 13 atoms in size, apparently ruling out the possibility that the reaction takes place over small oxidic clusters.

REFERENCES

1. Tsubota, S., Haruta, M., Kobayashi, T., Ueda, A., and Nakahara, Y., *in* "Preparation of Catalyst V," p. 695. Elsevier, Amsterdam, 1991.
2. Haruta, M., Tsubota, S., Kobayashi, T., Kageyama, H., Genet, M. J., and Delmon, B., *J. Catal.* **144**, 175 (1993).

3. Cunningham, D. A. H., Kobayashi, T., Kamijo, N., and Haruta, M., *Catal. Lett.* **25**, 257 (1994).
4. Haruta, M., *Catal. Today* **36**, 153 (1997).
5. Hayashi, T., Tanaka, K., and Haruta, M., *in* "211th meeting of the Am. Chem. Soc. Symposium on Heterogeneous Hydrocarbon Oxidation, New Orleans, 1996." (B. Warren and T. Oyama, Eds.), p. 71.
6. Debye, P., *Ann. Phys.* **46**, 807 (1915).
7. Gnutzmann, V., and Vogel, W., *J. Phys. Chem.* **94**, 4991 (1990).
8. Vogel, W., Rosner, B., and Tesche, B., *J. Phys. Chem.* **97**, 11611 (1993).
9. Vogel, W., Sachtler, W. M. H., and Zhang, Z., *Ber. Bunsenges. Phys. Chem.* **97**, 280 (1993).
10. Hartmann, N., Imbihl, R., and Vogel, W., *Catal Lett.* **28**, 373 (1994).
11. Vogel, W., and Duff, D. G., *Langmuir* **11**, 401 (1995).
12. Kazakov, A. V., Shapiro, E. S., and Voskoboinikov, T. V., *J. Phys. Chem.* **99**, 8323 (1995).
13. Hall, B. D., Flueli, R., Monot, R., and Borel, J. P., *Z. Phys. D, At. Mol. Clusters* **12**, 97 (1989).
14. Vogel, W., Cunningham, D. A. H., Tanaka, K., and Haruta, M., *Catal. Lett.* **40**, 175 (1996).
15. Mackay, A. L., *Acta. Crystall.* **15**, 916 (1962).
16. Uppenbrink, J., and Wales, D. J., *J. Chem. Phys.* **96**, 8520 (1992).
17. Buffat, P. A., Flüeli, M., Spycher, R., Stadelmann, P., and Borel, J. P., *Faraday Discuss.* **92**, 173 (1991).
18. Sawada, S., and Sugano, S., *NATO ASI Ser. Serc.* **1**, 119 (1992).
19. Sawada, S., and Sugano, S., *in* "Physics and Chemistry of Finite Systems: From Clusters to Crystals" (P. Jena, S. N. Khanna, and B. K. Rao, Eds.), Vol. 1, p. 119. Kluwer, Holland, 1992.
20. Kumar J., and Gupta, A., *in* "Physics and Chemistry of Finite systems: from Clusters to Crystals" (P. Jena, S. N. Khanna, and B. K. Rao, Eds.), Vol. 1, p. 93. Kluwer. Holland. 1992.
21. D'Agostino, G., Pinto A., and Mobilio, S., *Phys. Rev. B* **48**, 14447 (1993).
22. Patil, A. N., Paithankar, D. Y., Otsuka, N., and Andres, R. P., *Z. Phys. D* **26**, 135 (1983).
23. Tsubota, S., Yamada, N., Haruta, M., Kobayashi, T., and Nakahara, Y., *Chem. Express* **5**, 349 (1990).
24. Sham, T. K., Yiu, Y. M., Kuhn, M., and Tan, K. H., *Phys. Rev B* **41**, 11881 (1990).
25. Koningsberger, D. C., and Prins, R., "X-ray Absorption: Principles, Applications, Techniques of EXAFS SEXAFS, and XANES," Chemical Analysis, Vol. 92. Wiley, New York, 1988.
26. Hansen, L. B., Stoltze, P., Nørskov, J. K., Clausen, B. S., and Niemann, W., *Phys. Rev. Lett.* **64**, 3155 (1990).
27. Balerno, A., Bernieri, E., Picozzi, P., Reale, A., Satucci, S., Burattini E., and Mobilio, S., *Phys. Rev. B* **31**, 5058 (1985).
28. Cocco, G., Enzo, S., Fagherazzi, G., Schiffini, L., Bassi, I. W., Vlaic, G., Galvagno, S., and Parravano, G., *J. Phys. Chem.* **83**, 2527 (1979).
29. Balerna, A., and Mobilio, S., *J. Phys. C* **47**(8), 1009 (1986).
30. Bassi, I. W, Lytle, F. W., and Parravano, G., *J. Catal.* **42**, 139 (1976).
31. Bassi, I. W., Garbassi, F., Vlaic, G., Marzi, A., Tauszik, G. R., Cocco, G., Galvagno, S., and Parravano, G., *J. Catal.* **64**, 405 (1980).